

Synthesis and applications of composite cathode based on $\text{Sm}_{0.5}\text{Sr}_{0.5}\text{CoO}_{3-\delta}$ for solid oxide fuel cell

Young Min Park* and Haekyoung Kim**[†]

*Fuel Cell Project, Research Institute of Industrial Science and Technology, Pohang 790-330, Korea

**School of Materials Science & Engineering, Yeungnam University, Gyeongsan 712-749, Korea

(Received 2 May 2013 • accepted 31 July 2013)

Abstract—Cobaltite based perovskites, such as $\text{Sm}_{0.5}\text{Sr}_{0.5}\text{CoO}_{3-\delta}$ (SSC), are attractive solid oxide fuel cell (SOFC) cathodes due to their high electrochemical activity and electrical conductivity. To obtain higher fuel cell performance with smaller particles, nano-sized SSC powders were synthesized by a complex method with/without carbon black, HB170. However, during synthesis, carbon black reacted with Sr, and unfortunately formed SrCO_3 . To obtain pure perovskite SSC, a calcination temperature of 900 °C is needed. At 680 °C, an SOFC with SSC (calcined at 700 °C and synthesized without HB170) exhibited a higher fuel cell performance, of 0.68 W·cm⁻², than that with SSCHB (calcined at 900 °C and synthesized with HB170), of 0.58 W·cm⁻². Adding GDC for composite cathode is more effective in SSCHB porous cathodes than in SSC porous cathodes. At 680 °C, the composite cathode of SSCHB6-GDC4 exhibited the highest maximum power density of 0.72 W·cm⁻² which results from the combined effects of lowered charge transfer polarization and mass transfer polarization. To obtain higher fuel cell performance, optimum composition and processes are necessary.

Key words: Solid Oxide Fuel Cell, Inorganic Dispersant, Anode Supported Cell, Composite Cathode, $\text{Sm}_{0.5}\text{Sr}_{0.5}\text{CoO}_{3-\delta}$

INTRODUCTION

Solid oxide fuel cells (SOFCs) are considered an efficient and environmentally friendly power generation system for power plants and distributed power. However, the high operating temperature limits the selection of materials and the long-term stability of materials and components, which motivates a reduction in operating temperature of SOFCs. However, ohmic and polarization resistances increase when the operation temperature decreases, which decreases fuel cell performance. The $\text{La}_{1-x}\text{Sr}_x\text{MnO}_3$ (LSM)-based cathode is a commonly used cathode material for high temperature SOFCs, but it performs poorly because of sluggish oxygen reduction reaction (ORR) kinetics, which causes the cell to have a low current capacity when the operating temperature of a SOFC single cell is below 800 °C. Hence, considerable efforts are being made to develop a new class of perovskite-based cathode material for SOFCs that have mixed ionic and electronic conductivity with high electro-catalytic activity in oxygen reduction and relatively lower operating temperature (600–800 °C) [1–11]. Among these, cobaltite based perovskites, such as $\text{La}_{0.5}\text{Sr}_{0.5}\text{CoO}_{3-\delta}$ (LSC), $\text{Sm}_{0.5}\text{Sr}_{0.5}\text{CoO}_{3-\delta}$ (SSC), $\text{La}_{0.5}\text{Sr}_{0.5}\text{Co}_{0.2}\text{Fe}_{0.8}\text{O}_{3-\delta}$ (LSCF), and $\text{Ba}_{0.5}\text{Sr}_{0.5}\text{Co}_{0.8}\text{Fe}_{0.2}\text{O}_{3-\delta}$ (BSCF), are attractive due to their high electrochemical activity and electrical conductivity [12–19]. A composite cathode with BSCF exhibits better electronic conductivity than that of pure BSCF [20]. SSC compounds show higher ionic conductivity than LSC [13,21,22], and are a good catalyst for oxygen reduction [23]. However, the disadvantages of SSC are its large thermal expansion coefficient and high reactivity

with YSZ electrolyte above 900 °C [22]. A dense or porous interlayer such as GDC and SDC has been used to reduce the mismatch and prevent reactions between the cathode and YSZ electrolyte [24,25].

The electrochemical performance of anode-supported SOFCs can also be varied by manipulating the processing and micro-structural parameters of the cathode materials [5,26]. The small-particle-size and high-surface area of the nanocrystalline materials are favorable in the SOFC cathode electrode [27–29], which results in enhancement of the electro-catalytic reduction of the oxidant, along with higher catalytic activity [30–32]. Nanocrystalline cathodes can be easily sintered and the extent of sinterability of these powders can be controlled by the amount of organic binder added during the preparation of the thick film paste for screen-printing. Nevertheless, the high temperatures involved for phase formation of the SOFC cathode materials hinder the formation of nanostructures [32–34]. In previous work [35], $\text{La}_{0.5}\text{Sr}_{0.5}\text{Co}_{0.2}\text{Fe}_{0.8}\text{O}_{3-\delta}$ (LSCF) was synthesized by a complex method with an inorganic nano-dispersant, carbon black, which resulted in smaller particle size and lower sintering temperature, for achieving higher fuel cell performance.

We prepared SSC-based nanocrystalline powders by a complex method with ethylene diamine tetra-acetic acid (EDTA) and citric acid as chelants to reduce the phase formation temperature. Carbon black, an inorganic nano-dispersant, was also used to control the size of nanocrystalline SSC. The SSC-based cathode powders synthesized with carbon black were characterized for structural, thermal, and electrical properties and compared with a powder synthesized without carbon black. The electrochemical performance of the Ni-YSZ support/Ni-YSZ anode functional layer/YSZ electrolyte/GDC interlayer anode-supported SOFC cells was evaluated with synthesized SSC cathode materials.

^{*}To whom correspondence should be addressed.
E-mail: hkkim@ynu.ac.kr

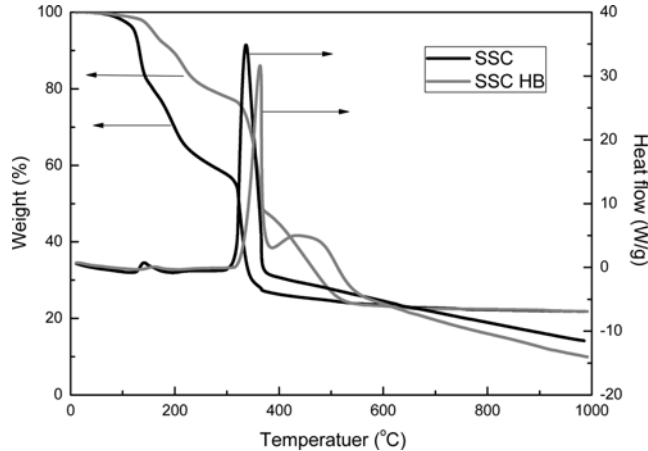


Fig. 1. Thermal behavior of synthesized $\text{Sm}_{0.5}\text{Sr}_{0.5}\text{CoO}_{3-\delta}$.

EXPERIMENT

Starting materials used included $\text{Sm}(\text{NO}_3)_3 \cdot 6\text{H}_2\text{O}$ (4.440 g, 0.01 mol), $\text{Sr}(\text{NO}_3)_2$ (2.116 g, 0.01 mol) and $\text{Co}(\text{NO}_3)_2 \cdot 6\text{H}_2\text{O}$ (5.821 g, 0.02 mol) all in analytical grades. They were dissolved in 100 ml of deionized water to prepare a homogeneous nitrate solution. Then, ethylenediaminetetraacetic acid (EDTA, 5.845 g, 0.04 mol) powders and citric acid (7.645 g, 0.02 mol) were added for chelating into a homogeneous nitrate solution. The solution was heated in a water bath at 70 °C. After getting a clear solution, HI BLACK170 (HB170, low color furnace carbon black), 5 g, which has a surface area of

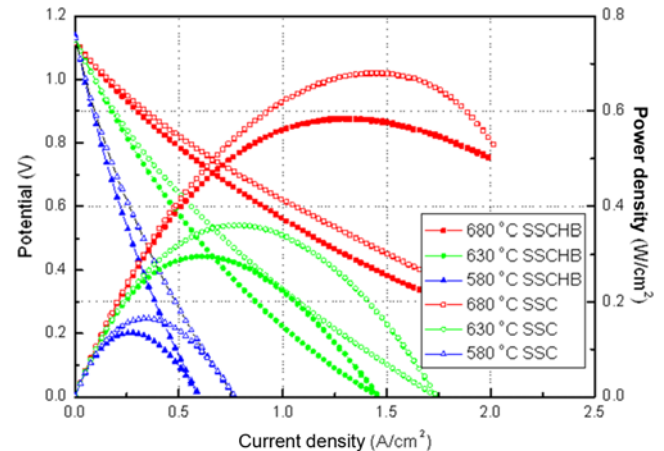


Fig. 4. Fuel Cell Performance of SOFCs with SSC based cathodes.

$23 \text{ m}^2 \cdot \text{g}^{-1}$ and particle size of 58 nm, was added as an inorganic nano-dispersant. After obtaining a transparent solution, the mixture was continuously heated to evaporate the water until the magnetic bar stopped rotating. The remaining mixture was dried at 80–120 °C in a vacuum oven overnight to remove residual water. The dried powders were crushed and calcined at 500–900 °C for 3 hours to form a perovskite phase, removing the organic compounds and inorganic nano-dispersants. Thermogravimetric analysis (TGA) was carried out on the crushed powders from room temperature to 1,000 °C in air at a heating rate of $3 \text{ °C} \cdot \text{min}^{-1}$ using a Shimadzu TA-50 thermal analyzer to investigate the thermal behavior. The calcined powders

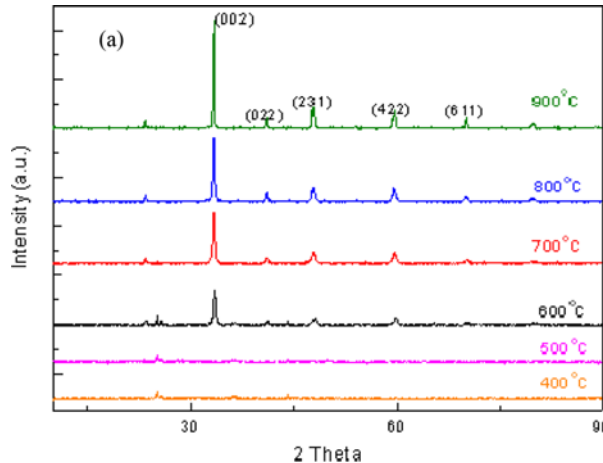


Fig. 2. XRD spectra of powders calcined at various temperatures (a) SSC (synthesized without HB170).

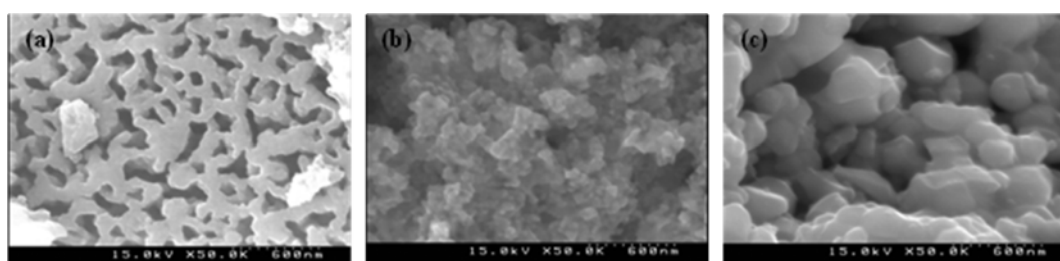
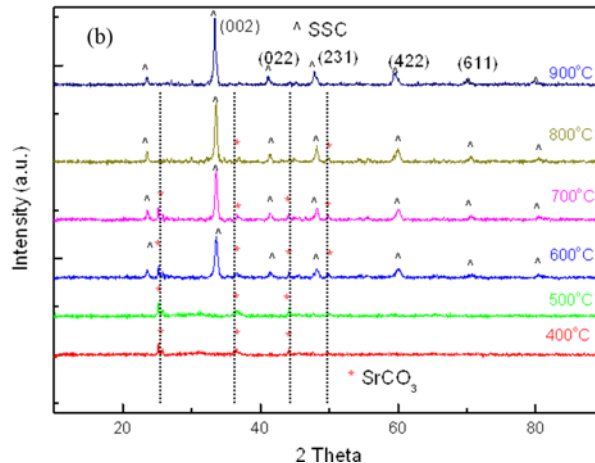


Fig. 3. SEM images of (a) SSC calcined at 700 °C, (b) SSCHB calcined at 700 °C, and (c) SSCHB calcined at 900 °C.

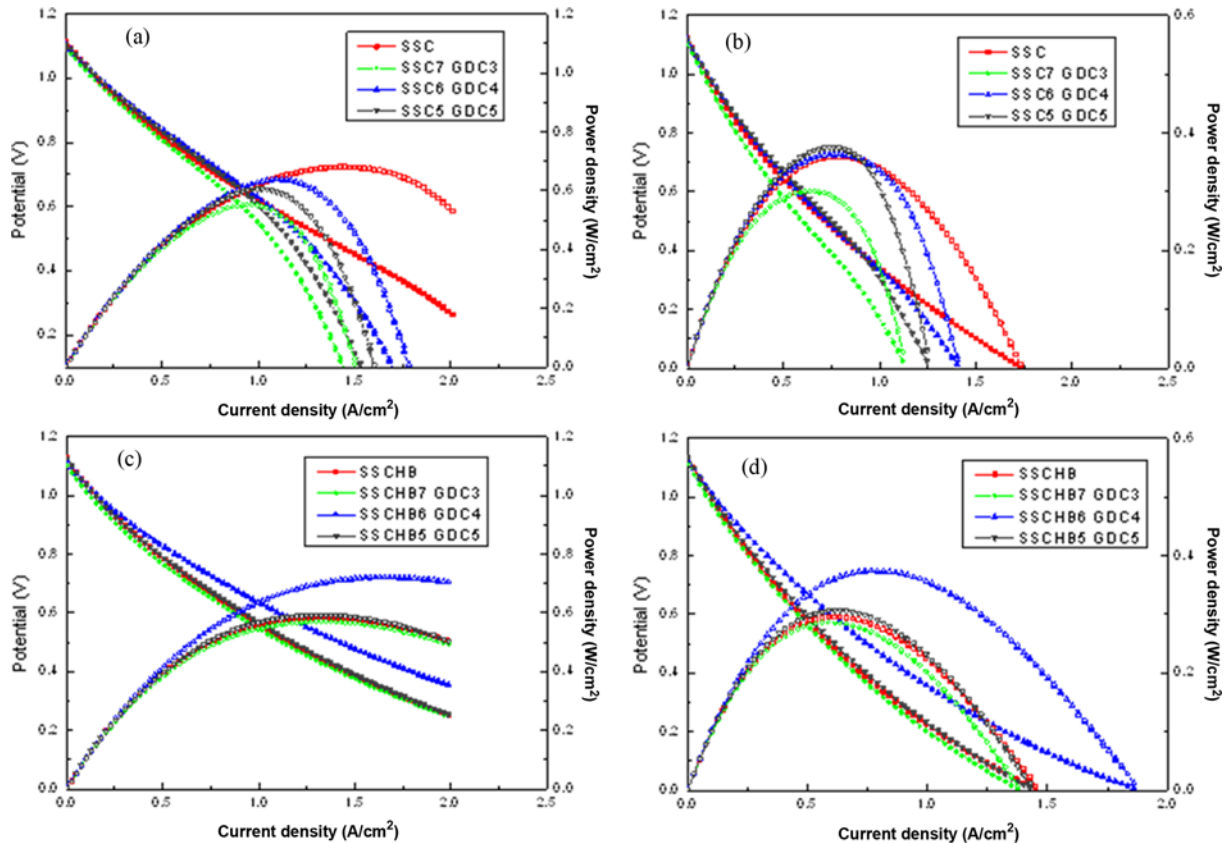


Fig. 5. Fuel cell performance of composite cathode based on SSC and SSCHB.

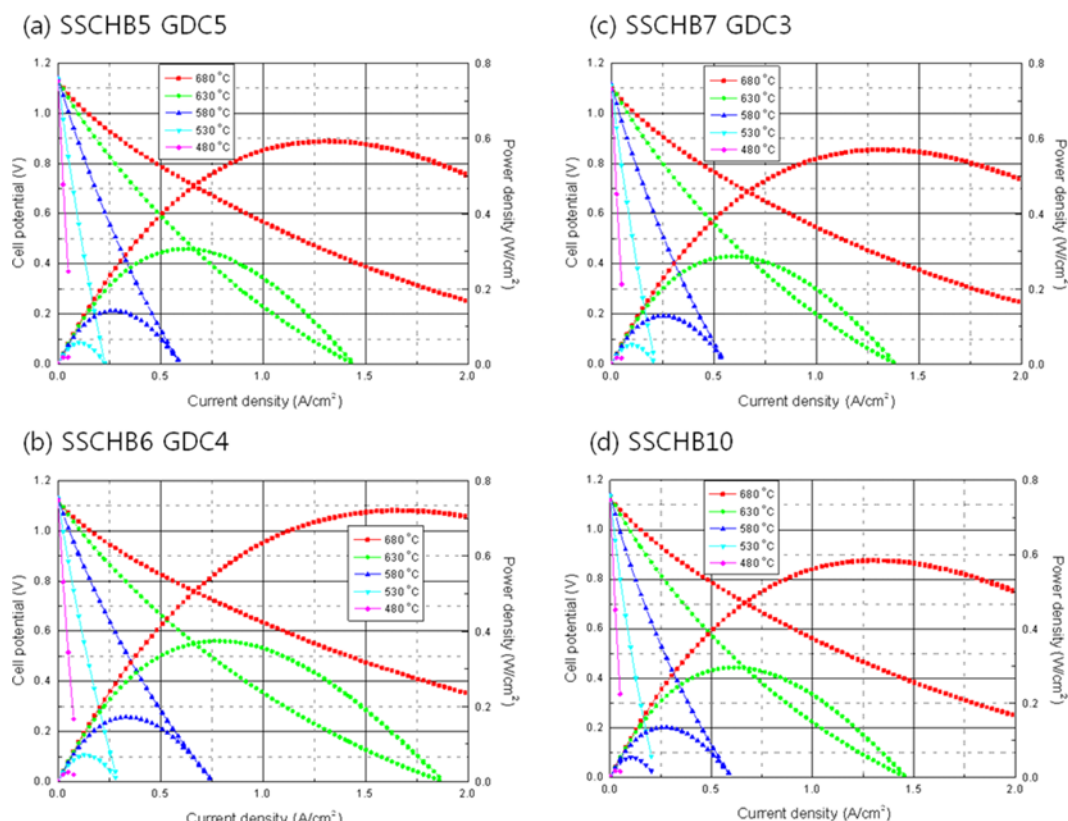


Fig. 6. Fuel cell performance of composite cathode based on SSCHB with temperature.

were characterized by means of X-ray diffraction and scanning electron microscopy (SEM) to observe the phases and morphologies.

To characterize the fuel cell performance, anode-supported cells (ASC), which consist of Ni-YSZ of 900 μm as a support layer, Ni-YSZ of 20 μm as an anode functional layer (AFL), YSZ of 10 μm as an electrolyte and GDC of less than 1 μm , were fabricated by

using a tape casting and co-firing method at 1,370 °C, and aerosol deposition method. The anode-supported cells were cut into circles with diameters of 2.6 cm from a 25 cm \times 25 cm plate. Cathode pastes were prepared from synthesized SSC powders and GDC powder with 50 wt% organic binder solution and screen-printed on the Ni-YSZ/YSZ/GDC anode-supported cell. The composite cathodes con-

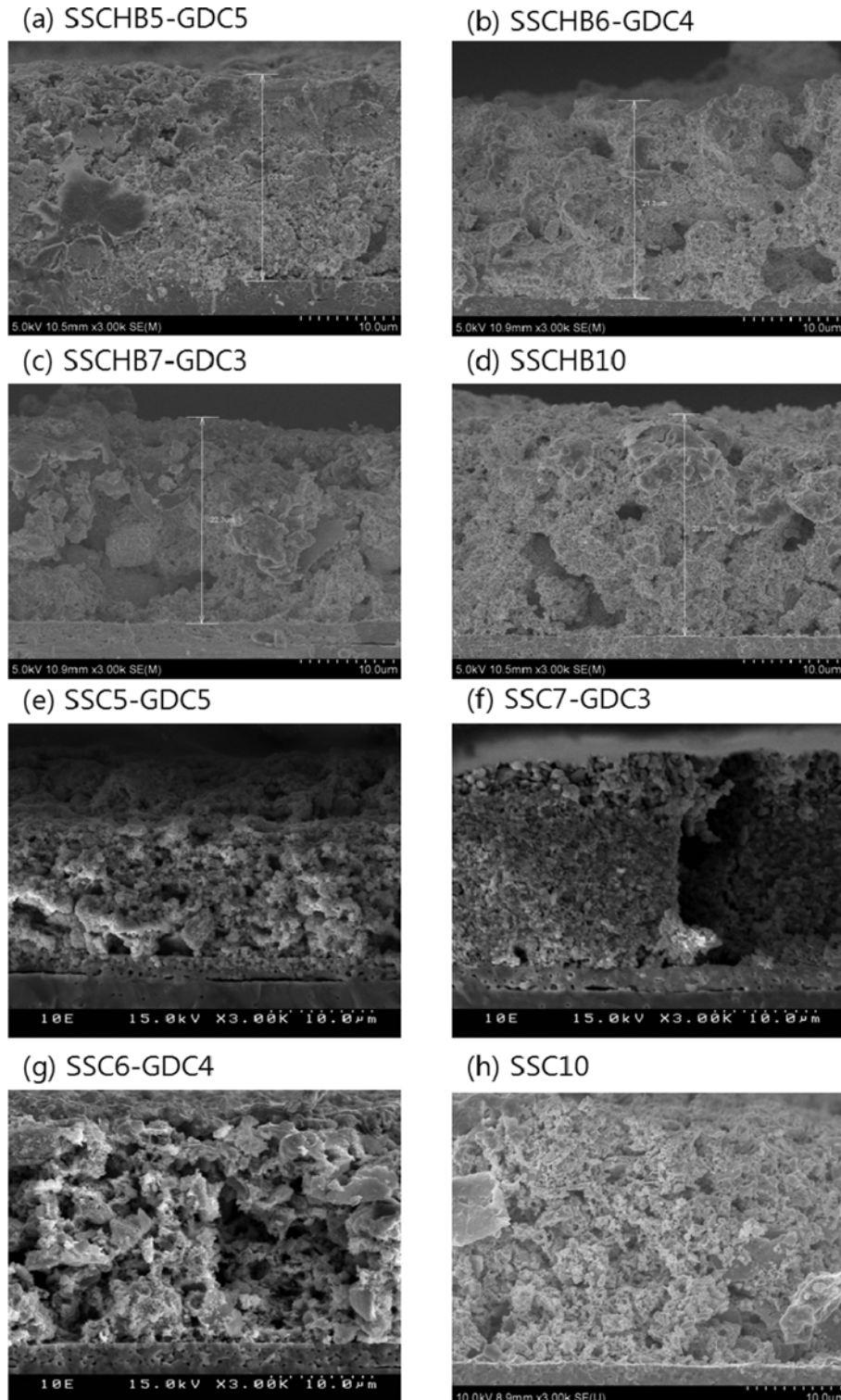


Fig. 7. Cross-sectional images of SOFCs.

sist of SSC or SSCHB with GDC with a weight ratio 5 : 5 to 7 : 3. SSC calcined at 700 °C, and SSCHB calcined at 900 °C were used as cathode materials. SOFCs with SSCHB cathodes synthesized with HB170, and SSC cathodes synthesized without HB170 were sintered at 700 °C. The active cathode area was 0.785 cm².

The fabricated cells were assembled and sealed with Ceramabond 571 from AREMCO in a jig to measure current-voltage characteristic and impedances. Pt paste and mesh were used for current collecting. The SOFCs were heated and anode reduction was performed with 300 cc·min⁻¹ of 97% H₂ - 3% H₂O for 3 h. Fuel cell performance was measured at each temperature with 300 cc·min⁻¹ of 97% H₂ - 3% H₂O and 1,000 cc·min⁻¹ of air. The impedances were measured with the WEIS system from Wonnatech. The impedance spectra were obtained in the frequency range of 100 kHz to 0.1 Hz with applied AC voltage amplitude of 100 mV at each temperature and open circuit voltage. After electrochemical measurements, the SOFC microstructures were characterized with scanning electron microscopy, using JSM-6480LV.

RESULTS AND DISCUSSION

The thermal analysis curves of the crushed powders are presented in Fig. 1. Significant weight losses in the SSC synthesized without HB170, coded as SSC, are observed at ~175 °C and 300 °C due to the decomposition of organic compounds, citric acid, and EDTA. Above 400 °C, no significant weight loss is observed and the heat flows for phase formation are characterized. However, the SSC synthesized with HB170, coded as SSCHB, has additional weight losses at 400–450 °C due to the decomposition of the HB170. Above 500 °C, weight loss is not observed and the heat flows for phase formation

are characterized. The organic chelants and HB170 decompose under 500 °C, which means that all impurities are decomposed during the calcination process of the nanocrystalline SSC. From the XRD analysis, shown in Fig. 2(a) of SSC without HB, SSC perovskite peaks appear from 600 °C, and the peaks get sharper and narrower as the calcination temperature increases. However, in Fig. 2(b) of SSC with HB, SrCO₃ peaks appear with SSC perovskite peaks from 600 °C. The pure SSC perovskite was obtained when SSCHB was calcined above 900 °C. The phases of SrCO₃ are formed with the reaction of Sr and excess carbon from HB170. However, SrCO₃ is not observed through the high temperature heat treatment, which can convert into CO₂ with air [36].

The morphologies of SSC calcined at 700 °C and SSCHB calcined at 700 °C and 900 °C are shown in Fig. 3. Fig. 3(b) shows sheets of small particles. When the calcination temperature increases to 900 °C, the agglomerations of SSCHB are easily observed in Fig. 3(c). When HB170 is used as inorganic nano-dispersant, small particles of SSC can be obtained. However, the impurities of SrCO₃ are present. In previous work with LSCF, HB170 was very favorable in synthesizing nanocrystalline powder with no impurities [35]. However, in the case of SSC, carbon black, HB170, was ineffective due to the impurity of SrCO₃.

The fuel cell performance of SOFCs with SSC (calcined at 700 °C) and SSCHB (calcined at 900 °C) is shown in Fig. 4. The SOFC with SSC exhibits higher fuel cell performance than that of SSCHB. SOFC with SSC shows 0.54 A·cm⁻², 0.27 A·cm⁻² and 0.14 A·cm⁻² at 680 °C, 630 °C and 580 °C, respectively. The current densities of SOFC with SSCHB are 0.47 A·cm⁻², 0.26 A·cm⁻² and 0.12 A·cm⁻² at 680 °C, 630 °C and 580 °C, respectively. With the BET measurement, the surface area of SSC is 3.44 m²·g⁻¹ and SSCHB is 0.99 m²·g⁻¹. The

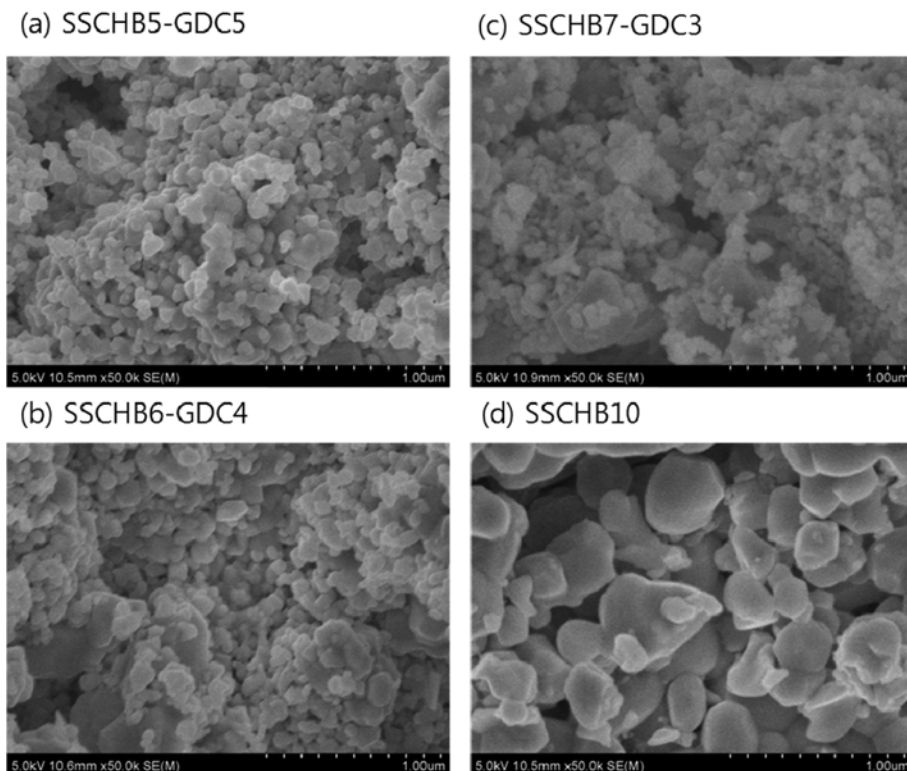


Fig. 8. Images of cathode in SOFCs.

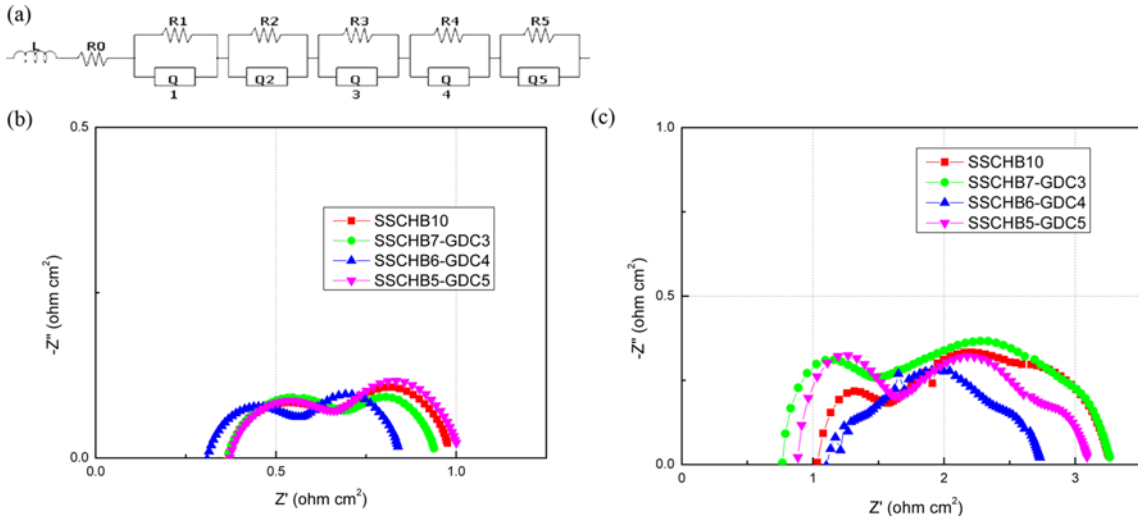


Fig. 9. (a) Equivalent circuits for impedance analysis, (b) Impedance spectra of SOFCs with SSCHB based composite cathodes at 680 °C, (c) Impedance spectra of SOFCs with SSCHB based composite cathodes at 580 °C.

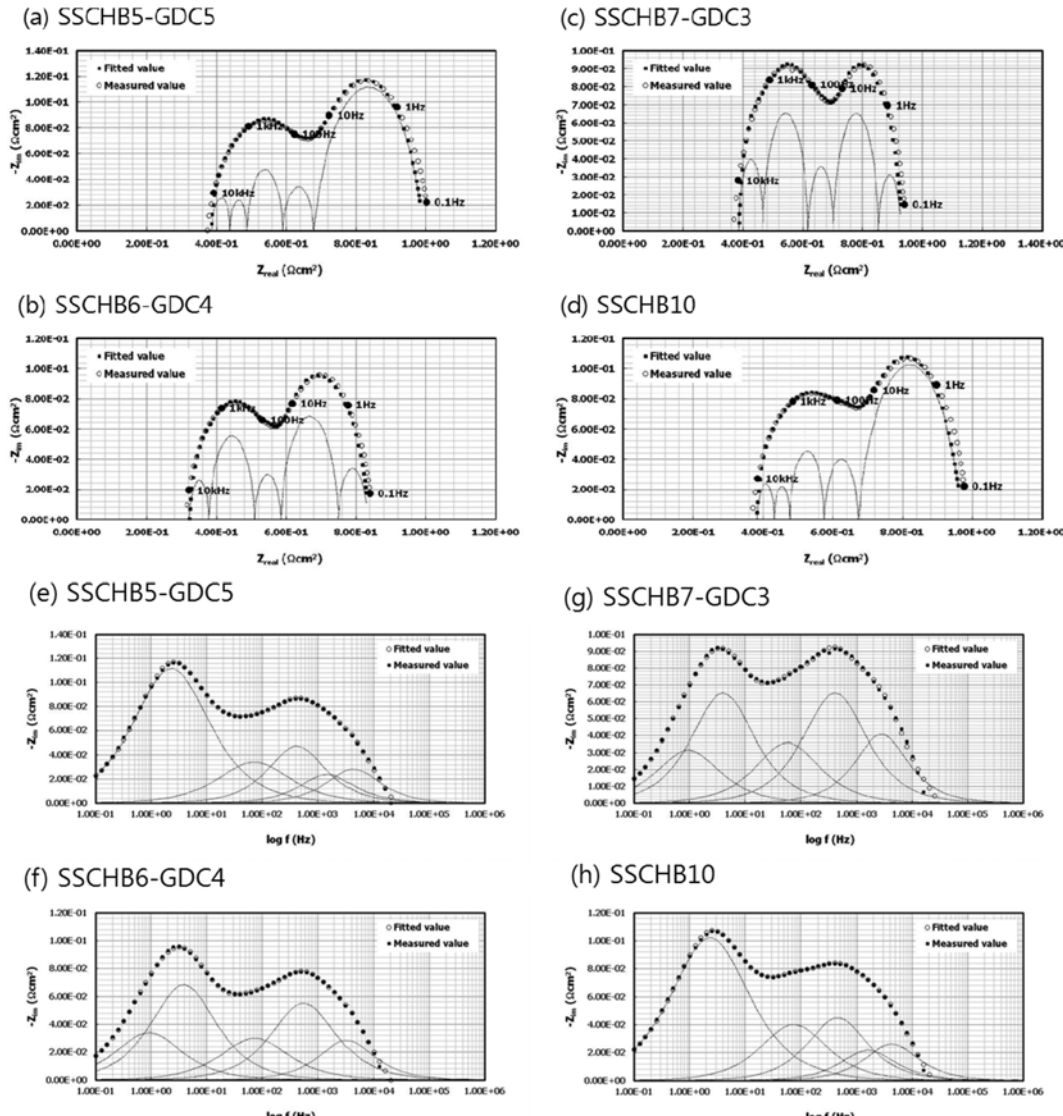


Fig. 10. Impedance spectra and bode plots at 680 °C.

higher SSC surface area, compared to SSCHB, results in the higher fuel cell performance.

Here, to obtain higher fuel cell performance, the composite cathodes were fabricated with GDC particles. The composite cathodes have varied ratios of SSC or SSCHB to GDC particles: the codes such as SSC (or SSCHB) X - GDC Y. SSC (or SSCHB) X - GDC (10-X) mean that the sum of SSC (or SSCHB) and GDC is 10. SSC10 and SSCHB10 are cathodes without GDC particles. The fuel cell performance of composite cathodes based on SSCHB and SSC is shown in Fig. 5 and Fig. 6. The electrochemical performance of porous cathodes is expected to be improved by adding GDC, as a result of the coarsening resistance of the cathode particles, thereby maintaining their porosity and triple phase boundaries (TPB) length. The effects of adding GDC are effective in the SSCHB porous cathode. By adding GDC, the SOFC with SSCHB6-GDC4 shows the highest values. SOFC with SSCHB6-GDC4 exhibits the higher maximum power densities, of $0.72 \text{ W} \cdot \text{cm}^{-2}$, $0.37 \text{ W} \cdot \text{cm}^{-2}$ and $0.17 \text{ W} \cdot \text{cm}^{-2}$ at 680°C , 630°C , and 580°C , respectively. However, in the case

of SSC, the addition of GDC to a SSC cathode is not beneficial for increasing fuel cell performance. The composite cathodes based on SSC, (SSC7-GDC3, SSC6-GDC4, and SSC5-GDC5) show the similar fuel cell performances, as shown in Fig. 5. SOFC with SSC7-GDC3 shows lower fuel cell performance with adding GDC. The lower surface area of SSCHB is more favorable to achieve incrementally enhanced electrochemical performance from the addition of GDC. As shown in Fig. 7, the SOFC cross-sectional images show the similar thickness of the cathodes with $20\text{-}23 \mu\text{m}$, which can exclude the effects of cathode thickness [37]. In the images of the SSCHB cathodes in Fig. 8, the addition of GDC is effective for coarsening resistance of the SSCHB particles, which affects the fuel cell performance.

To study the impedance, the equivalent circuit and the impedance spectra of the SOFC with composite cathodes based on SSCHB were obtained and are shown in Fig. 9. An equivalent circuit of the anode-supported SOFC has five impedance elements connected in series by distribution of relaxation time [38-40]. Based on the circuit, the impedances are modeled by five RQ elements. The fitting results

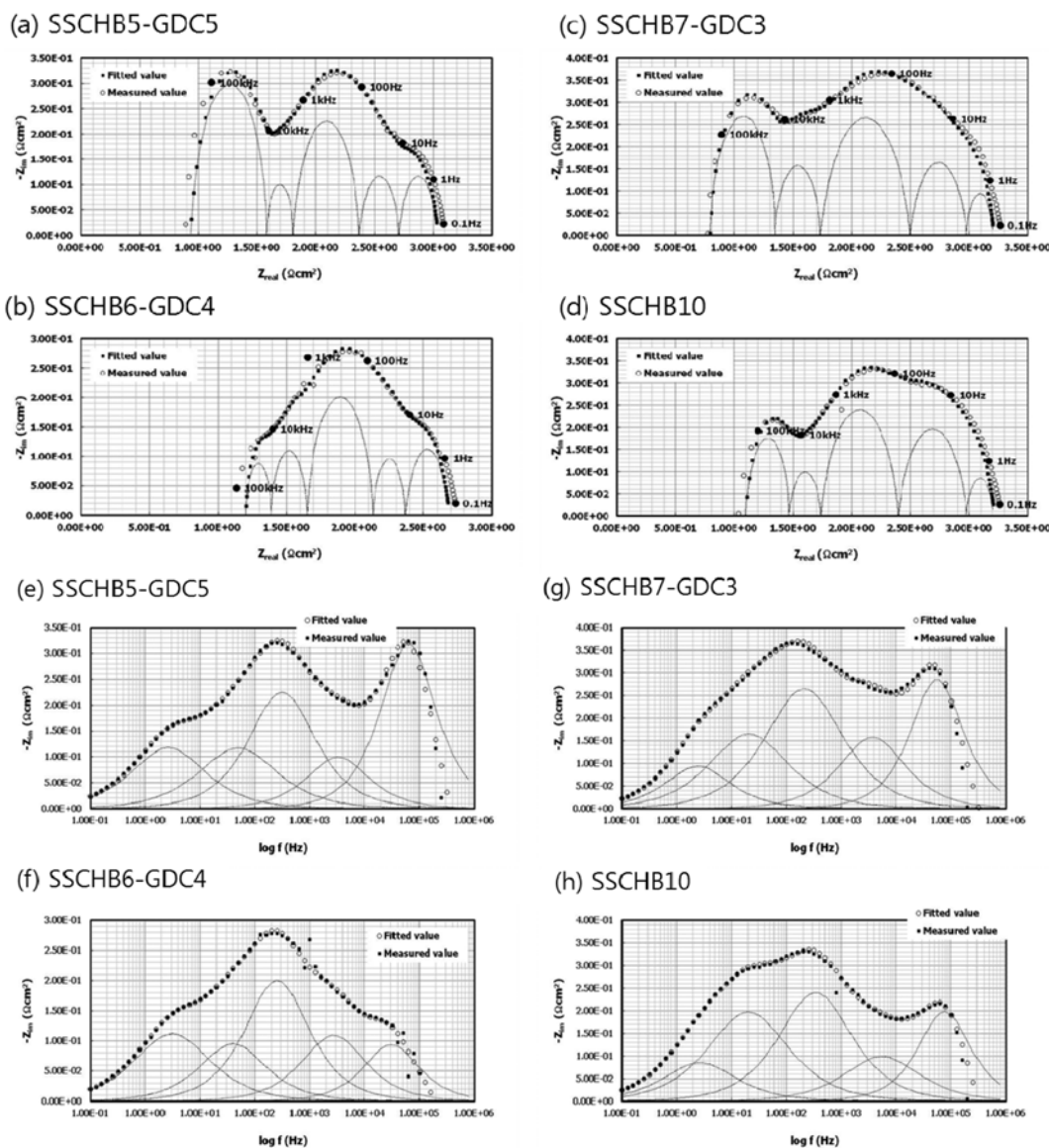


Fig. 11. Impedance spectra and bode plots at 580°C .

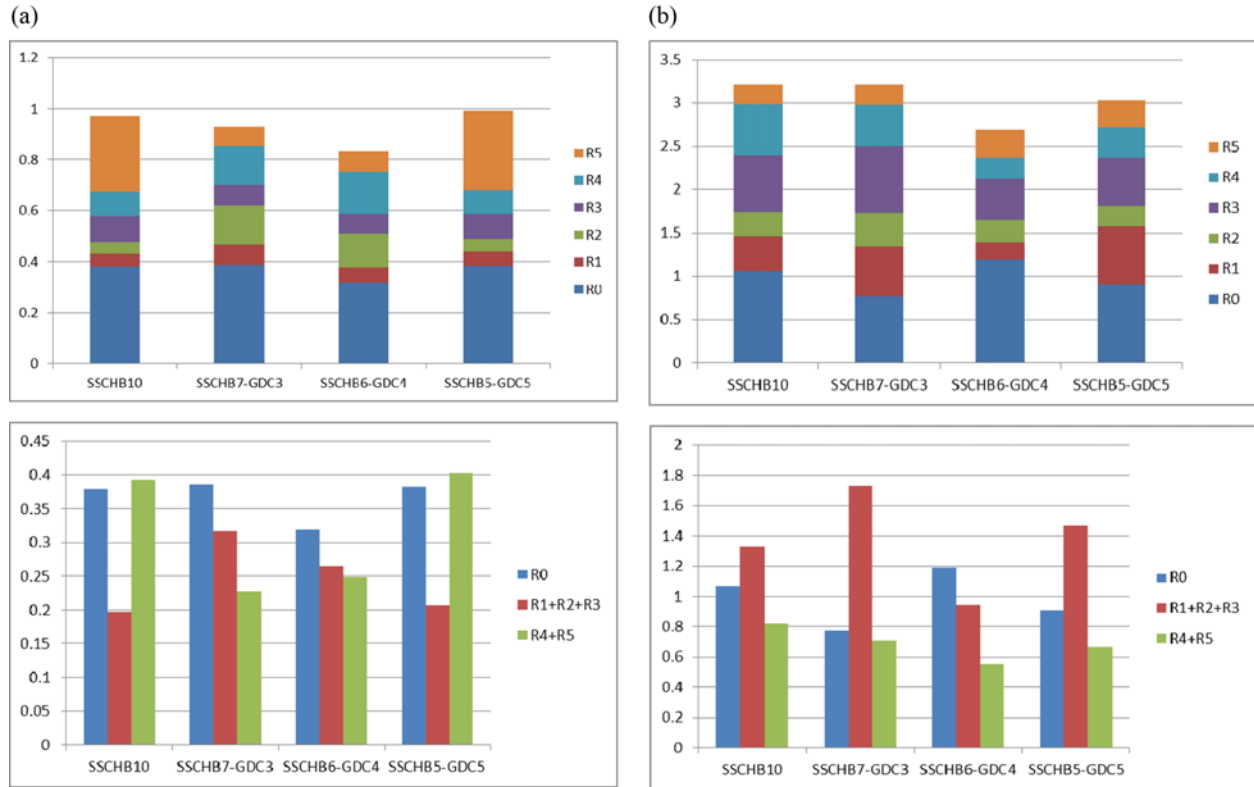


Fig. 12. Analysis of impedance fitting results. (a) 680 °C and open circuit voltage, (b) 580 °C and open circuit voltage.

of the composite cathodes open circuit voltage (OCV) at 680 °C and 580 °C are presented in Fig. 10 and Fig. 11, and the fitted results show good matching with the experimental data. R0 is from the ohmic resistance of the YSZ electrolyte, anode, composite cathode, GDC barrier, and connection wires; L is the inductance, which is attributed to the platinum current-voltage probes or the heating elements of the furnace used to heat the sample; (R1Q1) and (R3Q3) correspond to the gas diffusion coupled with the charge transfer reaction and ionic transport; (R2Q2) corresponds to the oxygen surface exchange kinetics and oxygen ion diffusivity at the cathode; (R4Q4) and (R5Q5) correspond to the gas diffusion reaction [39–43].

The analyses of impedance fitting results are shown in Fig. 12. The SOFC with the SSCHB6-GDC4 composite cathode exhibits the lowest ohmic resistance, and the lowest total resistance. The charge transfer polarization of the sum of R1, R2 and R3 is lower in SSCHB10 and SSCHB5-GDC5 than in SSCHB6-GDC4 and SSCHB7-GDC3. The mass transfer polarization of the sum of R4 and R5 is increased in SSCHB10 and SSCHB5-GDC5, resulting from the lower porosity. The mass transfer polarizations decrease in SSCHB6-GDC4 and SSCHB7-GDC3, resulting from their unchanged porosity.

Fuel cell performance depends on the ohmic resistance, charge transfer with TPB length, and mass transfer related to optimum porosity. Here, the addition of GDC to the porous SSCHB cathode results in combined effects on ohmic resistance, charge transfer, and mass transfer polarization, resulting from interfacial resistance, cathode conductivity, porosity, and TPB length. In the case of the composite with SSCHB and GDC, SSCHB6-GDC4 shows the best combined effect for ohmic resistance, charge transfer, and mass transfer polar-

ization. To obtain higher fuel cell performance, a design to achieve the optimum composition of perovskite and oxygen ion conductor and optimum processes is necessary.

CONCLUSIONS

We synthesized $\text{Sm}_{0.5}\text{Sr}_{0.5}\text{CoO}_{3-\delta}$ with a complex method using citric acid and EDTA with/without carbon black, inorganic nano-dispersants. In the calcination process, carbon black, HB170, resulted in an insulating phase of SrCO_3 via the reaction of Sr and the excess carbon of HB170. To get pure SSC, SSCHB needed to be calcined at 900 °C. At 680 °C, the SOFC with SSC (calcined at 700 °C and synthesized without HB170) exhibited a higher fuel cell performance, of 0.68 W cm^{-2} , than that of SSCHB (calcined at 900 °C), which was 0.58 W cm^{-2} . The higher surface area of SSC ($3.44 \text{ m}^2 \text{ g}^{-1}$), compared with SSCHB ($0.99 \text{ m}^2 \text{ g}^{-1}$), resulted in higher fuel cell performance. Here, to obtain higher fuel cell performances, the composite cathodes were fabricated with GDC particles. The addition of GDC was more effective in porous SSCHB cathodes than in SSC cathodes. SOFC with SSCHB6-GDC4 exhibited the highest fuel cell performance of 0.72 W cm^{-2} at 680 °C. The impedance spectra show that higher fuel cell performance results from the multiple effects of lowered ohmic resistance, higher porosity, and optimum charge transfer resistance of the GDC addition to porous SSCHB cathodes.

ACKNOWLEDGEMENTS

This work was supported by research grants from Yeungnam University in 2012.

REFERENCES

1. S. P. Jiang, *Solid State Ionics*, **146**, 1 (2002).
2. M. J. Jørgensen and M. Mogensen, *J. Electrochem. Soc.*, **147**, A433 (2001).
3. V. Dusastre and J. A. Kilner, *Solid State Ionics*, **126**, 163 (1999).
4. D. Kušcer, J. Holc, S. Hrovat and D. Kolar, *J. Eur. Ceram. Soc.*, **21**, 1817 (2001).
5. A. Mai, V. A. C. Haanappel, S. Uhlenbruck, F. Tietz and D. Stöver, *Solid State Ionics*, **176**, 1341 (2005).
6. A. Mai, V. A. C. Haanappel, S. Uhlenbruck, F. Tietz and D. Stöver, *Solid State Ionics*, **177**, 2103 (2006).
7. Y. Teraoka, H. M. Zhang, K. Okamoto and N. Yamazoe, *Mater. Res. Bull.*, **23**, 51 (1988).
8. J. Fleig, *J. Power Sources*, **105**, 228 (2002).
9. S. B. Adler, J. A. Lane and B. C. H. Steele, *J. Electrochem. Soc.*, **143**, 3554 (1996).
10. J. A. Kilner, R. A. De Souza and I. C. Fullarton, *Solid State Ionics*, **86-88**, 703 (1996).
11. J. Fleig, *Annu. Rev. Mater. Res.*, **33**, 361 (2003).
12. X. Zhang, M. Robertson, S. Yick, C. Dees-Petit, E. Styles, W. Qu, Y. Xie, R. Hui, J. Roller, O. Kesler, R. Maric and D. Ghosh, *J. Power Sources*, **160**, 1211 (2006).
13. S. Yang, T. He and Q. He, *J. Alloy Compd.*, **450**, 400 (2008).
14. Y. Guo, H. Shi, R. Ran and Z. Shao, *In. J. Hydrot. Energy*, **34**, 9496 (2009).
15. W. Zhou, Z. Shao, R. Ran and R. Cai, *Electron. Commun.*, **10**, 1647 (2008).
16. Y. L. Yang, C. L. Chen, S. Y. Chen, C. W. Chu and A. J. Jacobson, *J. Electrochem. Soc.*, **147**, 4001 (2000).
17. Y. Liu, W. Rauch, S. Zha and M. Liu, *Solid State Ionics*, **166**, 261 (2004).
18. E. P. Murray, M. J. Sever and S. A. Barnett, *Solid State Ionics*, **148**, 27 (2002).
19. Z. Shao and S. M. Haile, *Nature*, **431**, 170 (2004).
20. W. Zhu, Z. Lu, S. Li, B. Wei, J. Miao, X. Huang, K. Chen, N. Aif and W. Su, *J. Alloy Compd.*, **465**, 274 (2008).
21. H. Fukunaga, M. Koyama, N. Takahashi, C. Wen and K. Yamada, *Solid State Ionics*, **132**, 279 (2000).
22. H. Y. Tu, Y. Takeda, N. Imanishi and O. Yamamoto, *Solid State Ionics*, **100**, 283 (1997).
23. F. S. Baumann, J. Maier and J. Fleig, *Solid State Ionics*, **179**, 1198 (2008).
24. H. Jung, Y. Sun, H. Jung, J. Park, H. Kim, G. Kim, H. Lee and J. Lee, *Solid State Ionics*, **179**, 1535 (2008).
25. T. Suzuki, B. Liang, T. Yamaguchi, H. Sumi, K. Hamamoto and Y. Fujishiro, *J. Power Sources*, **199**, 170 (2012).
26. V. A. C. Haanappel, J. Mertens, D. Rutenbeck, C. Tropatz, W. Herzog, D. Sebold and F. Tietz, *J. Power Sources*, **141**, 216 (2005).
27. N. Gunasekaran, S. Saddawi and J. J. Carberry, *J. Catal.*, **159**, 107 (1996).
28. Y. Liu, H. T. Zheng, J. R. Liu and T. Zhang, *Chem. Eng. J.*, **89**, 213 (2002).
29. A. Dutta, J. Mukhopadhyay and R. N. Basu, *J. Eur. Cera. Soc.*, **29**, 2003 (2009).
30. S. Shukla, S. Seal, R. Vij and S. Bandyopadhyay, *Nano Lett.*, **3**, 397 (2003).
31. Q. S. Zhu and B. A. Fan, *Solid State Ionics*, **176**, 889 (2005).
32. M. G. Bellino, D. G. Lamas and N. E. WalsöedeReca, *Adv. Funct. Mater.*, **16**, 107 (2006).
33. W. Zhou, Z. P. Shao and W. Q. Jin, *J. Alloys Compd.*, **426**, 368 (2006).
34. L. Baqué, A. Caneiro, M. S. Morenó and A. Serquis, *Electron. Commun.*, **10**, 1905 (2008).
35. J. H. Kim, Y. M. Park and H. Kim, *J. Power Sources*, **196**, 3544 (2011).
36. H. Zhang, *Chinese J. Catal.*, **29**(1), 7 (2008).
37. F. Zhao and A. V. Virkar, *J. Power Sources*, **141**, 79 (2005).
38. A. Leonide, V. Sonn, A. Weber and E. Ivers-Tiffée, *ECS Transaction*, **7**(1), 521 (2007).
39. A. Leonide, V. Sonn, A. Weber and E. Ivers-Tiffée, *J. Electrochem. Soc.*, **155**(1), B36 (2008).
40. Y. M. Park, J. H. Kim and H. Kim, *Int. J. Hydrot. Energy*, **36**, 9169 (2011).
41. A. Weber, *International Symposium on Diagnostics Tools Fuel Cell Technologies* (2009).
42. H. Schichlein, A. C. Müller, M. Voigts, A. Krugel and E. Ivers-tiffée, *J. Appl. Electrochem.*, **32**, 875 (2002).
43. Y. M. Park, J. H. Kim and H. Kim, *Int. J. Hydrot. Energy*, **36**, 5617 (2011).